Astrophys Space Sci (2020) 365:48
https://doi.org/10.1007/s10509-020-03760-2

ORIGINAL ARTICLE

Global ionospheric maps forecasting based on an adaptive autoregressive modeling of grid point VTEC values

Cheng Wang[1,2] · Kaiyu Xue[2] · Zhipeng Wang[2] · Chuang Shi[1,2] · Lei Fan[1,2] · Tao Zhang[2]

Received: 26 July 2019 / Accepted: 2 March 2020

Abstract In the context of the International GNSS Service (IGS), the Ionosphere Associate Analysis Centers (IAACs) generate daily global ionospheric maps (GIMs). Time delays of at least one day for the daily GIMs product limit its value in real-time GNSS applications requiring high precision. Short-time forecasting of GIMs would be a good way to provide a basic background model for single-frequency GNSS users. We propose an improved algorithm for GIMs forecasting based on an adaptive autoregressive (AR) modeling of grid point vertical total electron content (VTEC) values (TVPG). We compare final daily GIMs (BUAG) with precise point positioning (PPP) derived VTEC values (PPPG) and JASON-2 VTEC values (J2TEC) to evaluate the performance of the TVPG and the GIMs based on the prediction of spherical harmonics coefficients (SHPG). The results of the comparison indicate that the TVPG have no obvious overestimate or underestimate with respect to BUAG. While, SHPG overestimates VTEC values in northern latitudes, and underestimates VTEC values in southern latitudes, by more than 2 TECU in some latitudes. Also, according to a comparison with PPPG and J2TEC, the TVPG is essentially better than the SHPG in middle and high latitudes at both low and high solar activity. However, it is worthy of further study to improve the performance of forecast GIMs in low latitudes.

Keywords Ionosphere · Forecasting · Autoregressive model · Total electron content

✉ Z. Wang
wangzhipeng@buaa.edu.cn

1 Research Institute of Frontier Science, Beihang University, No. 37 Xueyuan Road, Beijing 100083, China

2 School of Electronic Information Engineering, Beihang University, No. 37 Xueyuan Road, Beijing 100083, China

1 Introduction

The ionosphere is an important part of the near-Earth space. It is vital to national defense, aviation security, and the global navigation satellite system (GNSS) (Komjathy 1997; De Franceschi and Zolesi 1998; Schaer 1999). For single-frequency GNSS users, it is essential to correct the ionospheric delay errors, which could be as much as dozens of meters in the signal propagation direction. Some models, such as the International Reference Ionosphere (IRI) (Bilitza et al. 1992, 2011, 2017; Bilitza 2001; Bilitza and Reinisch 2008) and the NeQuick model (Nava et al. 2008; Nigussie et al. 2013), are suitable for the scientific analysis of the general trend of the ionosphere but are limited in practical applications since they are not highly accurate. The broadcast ionospheric models, like the Klobuchar model (Klobuchar 1987) as the official model for Global Positioning System (GPS) and the NeQuick G model (Angrisano et al. 2013; Prieto-Cerdeira et al. 2014) as the official model for Galileo, are quite useful for general navigation applications. However, the broadcast ionospheric models can only eliminate part of ionospheric delay errors in GNSS positioning. The network of the International GNSS Service (IGS) GNSS stations provides an opportunity for long-term monitoring of the ionosphere with high accuracy and good temporal and spatial resolution on a global scale. Since 1998, the Ionosphere Associate Analysis Centers (IAACs) of the IGS have been providing reliable global ionospheric maps (GIMs) (Hernández-Pajares et al. 2009). The centers are as follows: the Center for Orbit Determination in Europe (CODE) (Schaer 1999), the Jet Propulsion Laboratory (JPL) (Mannucci et al. 1998), the European Space Agency (ESA) (Feltens and Schaer 1998), the Technical University of Catalonia (Universitat Politècnica de Catalunya in Spanish, UPC) (Hernández-Pajares et al. 1999; Orús et al. 2005), Natu-

Published online: 05 March 2020

ral Resources Canada (NRCan), Chinese Academy of Sciences (CAS) (Li et al. 2015) and Wuhan University (WHU) (Zhang et al. 2013; Wang et al. 2016, 2018a). The GIM products are valuable for scientific analysis of the ionosphere and GNSS positioning in the post-processing phase.

However, the rapid and final GIMs are produced on a daily basis with latencies of at least one day up to one week or so. This latency limits applications of the daily GIMs for real-time GNSS positioning. For the last few years, several centers of IAACs have been studying real-time global ionospheric modeling. The real-time GIM products are still at the early testing stage, possibly due to the instability of the real-time GNSS data stream (Liu et al. 2018). Prediction of global ionospheric maps is a relatively reliable way for the correction of ionospheric delay errors in real-time GNSS applications. In addition, short-time predictions of GIMs could be used as a basic background model, thus allowing the real-time GIMs to achieve sub-meter accuracy for mass-market single-frequency users, such as automobiles, road mapping, and location-based services (García-Rigo et al. 2011).

In recent years, several methods have been studied for ionospheric forecasting, such as the autocorrelation method, the autoregressive moving average (ARMA) method (Krankowski et al. 2005), neural networks (Tulunay et al. 2006), and the autoregressive model (AR) method (Karthik et al. 2012). For forecasting global ionospheric maps a few centers of IAACs have provided one- and two-day-ahead GIMs for public access, since 2008 (ftp://cddis.gsfc.nasa.gov/). The CODE uses Least-Squares Collocation (LSC) to extrapolate the spherical harmonics (SH) coefficients to forecast GIMs (Schaer 1999). The UPC uses a Discrete Cosine Transform (DCT) technique to predict the GIMs (García-Rigo et al. 2011). Also, an adaptive autoregressive modeling (AARM) algorithm is developed for generating the predicted GIMs (Wang et al. 2018b). The AARM method is based on the extrapolation of SH coefficients to generate predicted GIMs. The first step of the AARM method is to predict independent SH coefficients of different degrees and orders. Then for the second step, the prediction of vertical total electron content (VTEC) at each grid point can be calculated using the predicted SH coefficients. However, there are twice accumulated errors in the forecast. The first one is the error of AR modeling of SH coefficients. The second one is the linear combination of the predicted SH coefficients for calculating VTEC predictions, which further enlarges the errors. In this study, we propose an improved method to forecast the ionosphere based on single-grid-point VTEC values. There is only once accumulated error for this method. The first section of this study is devoted to a detailed description of the improved method. The performance of proposed method is investigated by using several comparisons with final daily GIMs. In addition, external independent JASON VTEC values are introduced for testing the performance of predicted GIMs over oceans. Additionally, we compare the predicted GIMs with VTEC values derived from precise point positioning (PPP) with raw observations (Wang et al. 2020). The final daily GIMs are compared with JASON VTEC data and with PPP derived VTEC values as a reference. Finally, we present the conclusions in the last section.

2 Methodology of ionospheric forecasting

2.1 Daily GIMs from GPS measurements

In the context of the IGS, IAACs have been providing daily rapid and final GIM products since 1998 without interruption of scientific studies and applications. The global ionospheric VTEC maps are generated independently by the seven centers of IAACs, each using different methods, algorithms, and strategies (Hernández-Pajares et al. 2017; Roma-Dollase et al. 2018b). The JPL computes the VTEC maps with triangular tiles and introduces climatological models for generating GIMs products without gaps (Mannucci et al. 1998). The UPC uses a two-layer tomographic model and Kriging interpolation for improving GIMs products (Hernández-Pajares et al. 1999; Orús et al. 2005). The CODE proposed spherical harmonic (SH) expansion to represent the global ionospheric VTEC maps (Schaer 1999). The other centers (including EAS, NRCan, CAS, and WHU) use SH expansion as the main algorithm along with some improved methods to represent GIMs (Roma-Dollase et al. 2018b). The SH expansion is also used in this study for modeling the global ionosphere. The basic equation for ionosphere modeling with dual-frequency GNSS observations is given by Eq. (1):

$$\tilde{P}_1 - \tilde{P}_2 = I_1 - I_2 + c\,(DCB_r + DCB_s) + \Delta\varepsilon, \tag{1}$$

where $\tilde{P}_1$, $\tilde{P}_2$ are the carrier smoothed code measurements; c is the speed of light in vacuum; I_1 and I_2 are the ionospheric delay on the L1 and L2 signals; and DCB_r and DCB_s are the differential code biases (DCB) of receiver and satellite, respectively.

In addition, a mapping function is introduced to transform slant TEC (STEC) to VTEC. By ignoring the noise term Eq. (1) can be re-written as Eq. (2), where mf is the mapping function, which depends on the zenith distance z at the station; f_1 and f_2 indicate the carrier frequencies of the L1 and L2 signals; VTEC is the vertical TEC at the ionospheric pierce point (IPP):

$$\tilde{P}_1 - \tilde{P}_2 = \frac{40.3\left(f_2^2 - f_1^2\right)}{f_1^2 f_2^2} \cdot mf(z) \cdot VTEC + c(DCB_r + DCB_s). \tag{2}$$

The SH function represents VTEC referred to a solar geomagnetic frame as shown in Eq. (3):

$$VTEC(\varphi,\lambda)=\sum_{n=0}^{n_{max}}\sum_{m=0}^{n}\tilde{P}_{nm}(sin\varphi)(a_{nm}\cos(m\lambda)+b_{nm}\sin(m\lambda)), \quad (3)$$

where φ is the geomagnetic latitude of IPP; λ is the sun-fixed longitude of IPP; n and m are the degree and order of the model, respectively; $\tilde{P}_{nm}$ is the normalized associated Legendre function of degree n and order m; and a_{nm} and b_{nm} are the unknown SH coefficients to be estimated.

In this study, GPS observations from approximately 280 IGS stations are used for global ionospheric VTEC modeling. A minimum elevation cutoff of 10 deg. is chosen to avoid particularly noisy measurements. The model is based on a solar-geomagnetic reference frame with SH expansion to a degree and order of 15. One day of the GPS observations is divided into 24 sessions, with each session containing one hour of data. Groups of 25 SH parameters as well as DCBs of satellites and receivers can be estimated together by the least squares method. A zero-mean condition is imposed on all observed satellites, so that the DCB parameters of satellites and receivers can be separated. Once the SH coefficients are estimated, the VTEC value with a given latitude and longitude can be computed using Eq. (3). Then, daily GIMs products can be generated in the internationally adopted ionosphere exchange (IONEX) format. According to this format the GIMs contain the VTEC values of grid points from −87.5° to 87.5° latitude, in increments of 2.5°, and −180–180° longitude, in increments of 5°. Thus, there are 5183 grid points in each VTEC map. During the early years GIMs included 13 groups of VTEC maps at 2-hour intervals. Subsequently, more centers of IAACs began providing the daily GIMs with 25 groups of VTEC maps.

2.2 Forecasting global ionospheric maps

The autoregressive (AR) model has been widely used in forecasting of economics, geophysics, climate change, and global ionospheric maps (Cheng 1982; Gu and Jiang 2005; Weiss et al. 2012; Lee et al. 2016; Wang et al. 2018b). The basic principle of the AR model (Hamilton 1994) is presented as Eq. (4):

$$x_t=a_1x_{t-1}+a_2x_{t-2}+\cdots+a_px_{t-p}+\varepsilon_t, \quad (4)$$

where x_t is the time series; $[a_1,a_2,\ldots,a_p]$ is the vector of unknown AR coefficients, which can be estimated by least squares estimate (LSE); p is the order of the AR model; and ε_t is the zero-mean white noise. The usual strategy for one-step forecasting uses the estimated AR coefficients, as depicted in Eq. (5):

$$x_{n+1}=a_1x_n+a_2x_{n-2}+\cdots+a_px_{n-p}+\varepsilon_{n+1}, \quad (5)$$

where x_{n+1} is the forecasting parameter, n is the total number of the observed time series, and ε_{n+1} is the corresponding noise. For calculating one-day VTEC predictions at one grid point, a forecast would be performed 24 times by using Eq. (5).

The order p strongly determines the goodness-of-fit of the AR model and further influences the performance of the forecast. Several studies have adopted multiple a priori computations of the order, so as to select a predefined maximum order (Costa and Hengstler 2011). In this study, a predefined minimum order was proposed for AR modeling to avoid excessive computational cost. The F test was used to determine an adaptive order of the AR model. The formula of F-statistics is presented by Eq. (6):

$$F=\frac{(RSS_N-RSS_{N+1})/(f_N-f_{N+1})}{RSS_{N+1}/f_{N+1}}, \quad (6)$$

where RSS is the residual sum of squares; N is the predefined minimum order; and f is the degrees of freedom. In tests of the hypothesis, if the F-statistic is smaller than the critical value F_α, there is no significant difference between the two models. The lower order N would be selected for the AR model.

Although there's no theoretical criteria to determine the best length of the input time series so far, the corresponding impact could be minimized by using the adaptive AR model mentioned above. For the actual forecast of GIMs VTEC values 20 days are used to construct a dataset which has 481 $(20\times24+1)$ values. A predefined minimum order N of the AR model is selected to 60, which corresponds to 2.5 days of the time series of the VTEC values. A probability is set to 0.05, as a convenient cutoff level to reject the null hypothesis. This significance level of 0.05 is selected for calculating the critical value of the F distribution F_α. Once the adaptive order is determined, the VTEC values can be predicted using the estimated AR model. Since the VTEC characteristics of grid points vary significantly for different latitudes and longitudes, the VTEC values of each grid point should be predicted independently with respective time series that determine the adaptive order in the AR modeling. Consequently, the one-day-ahead forecast of global ionospheric VTEC maps would be generated in IONEX format. The following diagram, Fig. 1, shows the flow chart of global ionospheric maps forecasting based on the adaptive AR modeling of grid point VTEC values.

3 Results and analysis

3.1 Predicted GIMs and reference data

The rapid GIMs are generally produced in operational scenario, with the required rapid broadcast ephemeris which occasionally lacks the orbit information of several GNSS satellites. Also, the number of available IGS stations is limited

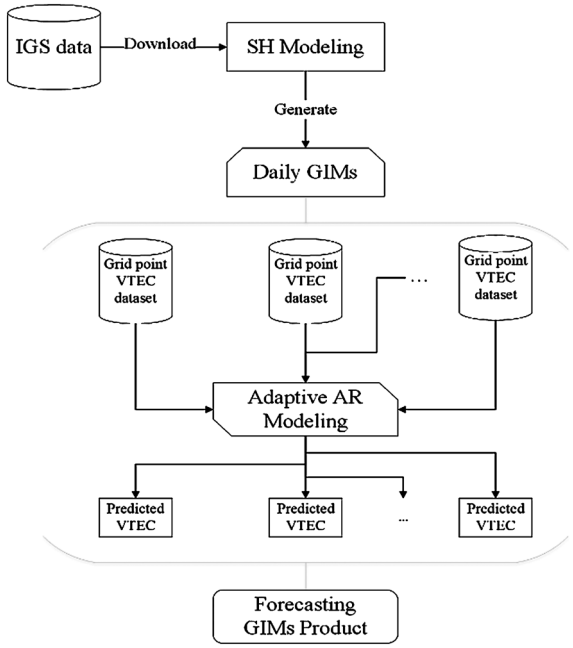

Fig. 1 Flow chart of GIMs forecasting based on the adaptive AR modeling of grid point VTEC values

Table 1 The differences among SHPG, TVPG and BUAG

	Type	Basic data	Method	Accumulated error
SHPG	forecast	SH coefficients	AR model	twice
TVPG	forecast	grid-point VTEC	AR model	once
BUAG	delay	GNSS observations	SH function	none

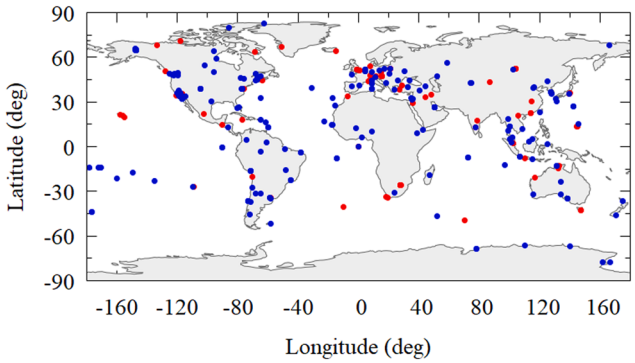

Fig. 2 Geographical distribution of the 280 IGS stations which provide daily GNSS observations for global ionospheric modeling (using the stations marked with both red and blue) and PPP derived VTEC calculation (using the stations marked with blue)

in short time (like within 1 day). Therefore, the accuracy of rapid GIMs is basically lower than that of final GIMs. So, we use the final GIMs as the fundamental input data for testing the proposed algorithm properly. According to the presented algorithms and method, we perform the SH modeling to generate the final daily GIMs (named BUAG), as well as the forecast for one-day-ahead GIMs (named TVPG) in 2009 and 2014. Another forecast GIMs (named SHPG) based on SH coefficients are also calculated as reference data. These two kinds of forecast GIMs are basically derived from the final daily modeling which could provide both SH coefficients and final GIMs (BUAG). The input data for forecast SHPG is the time series of estimated SH coefficients. Nevertheless, the time series of VTEC values at each grid point in BUAG constitutes the basic input data for forecast TVPG. Additionally, for TVPG, the forecast VTEC at each grid point could be directly calculated by using proposed AR model. However, the VTEC in SHPG wouldn't be computed until all SH coefficients have been predicted. As mentioned above in Sect. 1, the forecast SHPG have two steps which would enlarge the accumulated errors. The differences among these GIMs SHPG, TVPG and BUAG are presented in Table 1. We will compare two kinds of forecast GIMs (TVPG and SHPG) with daily GIMs BUAG to investigate the performance of the forecast. With development of precise orbit and clock determination precise point positioning (PPP) with undifferentiated and uncombined observations will retrieve slant ionospheric delays with high precision (Zhang et al. 2012). Some studies have demonstrated that the PPP solution could provide TEC values with greater precision than the traditional method of carrier-to-code leveling (Shi et al. 2012; Zhang et al. 2018). As independent reference data, PPP derived VTEC values (hereafter called PPPG) from more than 200 IGS stations (marked with blue in Fig. 2) are also introduced in this comparison. Additionally, JASON-2 VTEC measurements (hereafter called J2TEC) are collected as an external resource for testing the performance of both the forecast GIMs and final daily GIMs over the oceans. The comparison between forecast GIMs and other VTEC resources is conducted in terms of the average (bias) and root mean square (RMS) of the differences. Equation (7) and Eq. (8) show the calculation of bias and RMS values, where n is the total number of samples; and $VTEC_f$ and $VTEC_r$ are the forecast GIMs (TVPG and SHPG) and the reference VTEC resources (BUAG, PPPG, and J2TEC), respectively:

$$bias = \frac{1}{n}\sum_{i=1}^{n}(VTEC_f^i - VTEC_r^i) \tag{7}$$

$$RMS = \sqrt{\frac{\sum_{i=1}^{n}(VTEC_f^i - VTEC_r^i)^2}{n}}. \tag{8}$$

3.2 Comparison with final daily GIMs

Comparing the forecast GIMs and final daily GIMs is the most direct way to evaluate the proposed method. Several

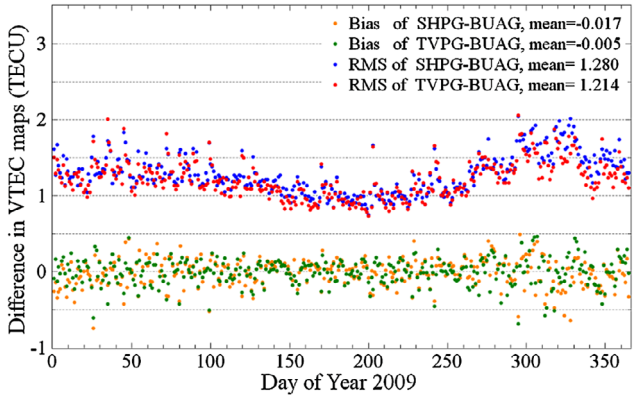

(a) Daily differences for comparison between forecast GIMs and BUAG in 2009

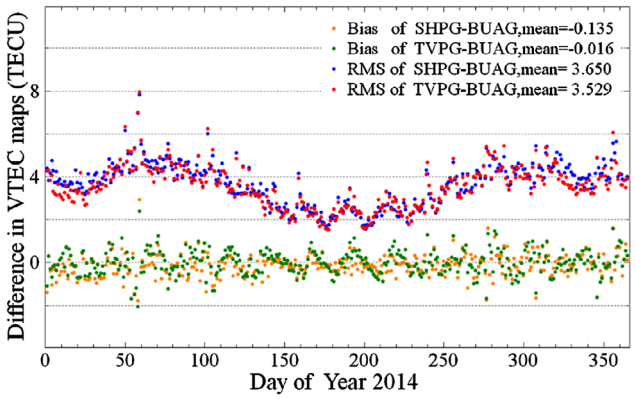

(b) Daily differences for comparison between forecast GIMs and BUAG in 2014

Fig. 3 Differences between the forecast GIMs (SHPG and TVPG) and final daily GIMs BUAG in 2009 and 2014

kinds of indices are calculated for comparison: the bias and RMS of the differences on a daily basis, a latitudinal basis, and a grid-point basis. The differences between forecast GIMs (SHPG and TVPG) and final daily GIMs BUAG are presented in Figs. 3–6. As seen from the bias values presented in Fig. 3, the annual means of the daily bias values both in 2009 and in 2014 are almost equal to zero. Note that in 2009, most of bias values are within a narrow distribution range of ±0.5 TECU. At high solar activity, a wider distribution range of bias values is still basically within ±2 TECU. The bias values indicate that the forecast GIMs have no apparent systematic bias with respect to final daily GIMs BUAG. Additionally, RMS values shown in Fig. 3 indicate that in 2009, there is an excellent consistency between forecast GIMs and BUAG, especially during northern summer when RMS values are less than one TECU. The annual averages of RMS values for comparison between forecast GIMs and BUAG in 2009 are less than 1.3 TECU. However, the annual averages are larger than 3.5 TECU in 2014. At the same time, there are some RMS values beyond six TECU on several days during northern spring at high solar activity. Generally, the performance of forecast GIMs is much better at low solar activity. Overall, the consistency between TVPG and BUAG is only slightly better than that between SHPG and BUAG.

Figure 4 shows more details of the differences in latitudes between the forecast GIMs (SHPG and TVPG) and final daily GIMs BUAG. The bias values for comparison between TVPG and BUAG are notably stable at zero in nearly all latitudes. SHPG overestimates VTEC values in northern latitudes, and underestimates VTEC values in southern latitudes, as compared to BUAG. Also, the differences are apparently larger in the Southern Hemisphere than those in the Northern Hemisphere, especially in mid-high southern latitudes at high solar activity. In addition, two groups of RMS values have a similar fluctuation from the southern latitudes to the northern latitudes. The consistency between forecast GIMs and BUAG is the best in middle and high latitudes of northern hemisphere, closely followed by the same latitudes of southern hemisphere, and is worst in the equatorial ionization anomaly (EIA) region. At low solar activity RMS values are generally less than two TECU in middle and high latitudes, except in the EIA region. While at high solar activity, the RMS values are less than four TECU in middle and high latitudes of the northern hemisphere, and larger than four TECU in the same latitudes of the southern hemisphere. The RMS values are larger than six TECU in the EIA region at high solar activity. Thus, the RMS values show that the discrepancies between the forecast GIMs and final daily GIMs are mainly concentrated in the low latitudes. The consistency between TVPG and BUAG in the EIA region is slightly lower than that between SHPG and BUAG. However, it is obviously that there is better consistency between TVPG and BUAG in middle and high latitudes than that between SHPG and BUAG at both low and high solar activity.

The grid-point bias of differences between forecast GIMs and BUAG in 2009 and 2014 are shown in Fig. 5. As the bias values presented in Fig. 5 indicate, it is obvious that SHPG overestimate VTEC values over eastern Asia and North Pacific Ocean and underestimate those in middle and high latitudes of Southern Hemisphere. At the same time the level of overestimating and underestimating is obviously higher at high solar activity than that in low solar activity. On the contrary, there is nearly no apparent overestimate or underestimate in TVPG, with only a very slight overestimate over a few parts of the North Pacific Ocean. This because the forecasting VTEC values of each grid-point is carried out independently. The forecasting VTEC values in TVPG have only once accumulated error without interfere with each other. However, the accumulated errors of predicted SH coefficients would affect all grid-point VTEC predictions. Therefore, SHPG shows a wide range of significant differences with respect to final GIMs (BUAG). Additionally, the RMS values in Fig. 6 show that there is an excellent consistency

GIMs BUAG in 2009 and 2014.

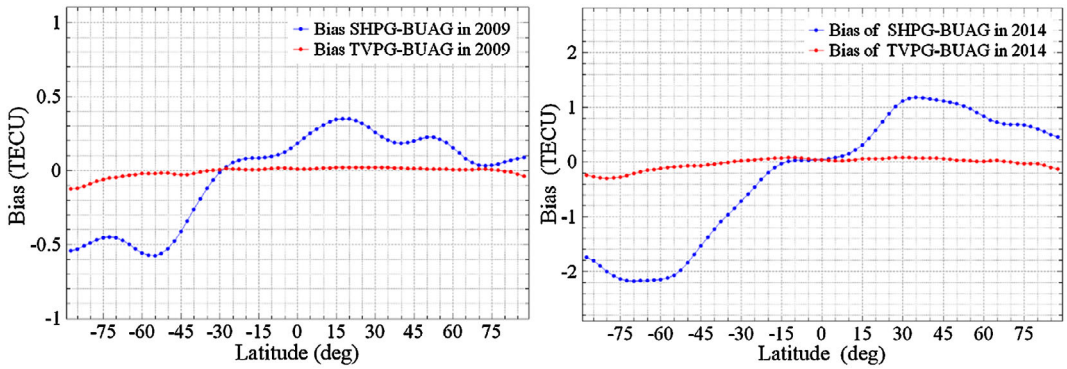

(a) Latitudinal bias for comparison between forecast GIMs and BUAG

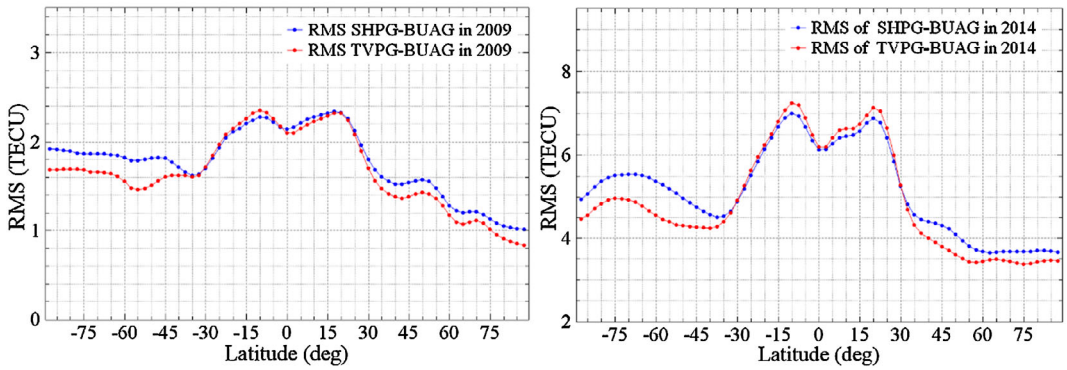

(b) Latitudinal RMS for comparison between forecast GIMs and BUAG

Fig. 4 Latitudinal differences between the forecast GIMs (SHPG and TVPG) and final daily GIMs BUAG in 2009 and 2014

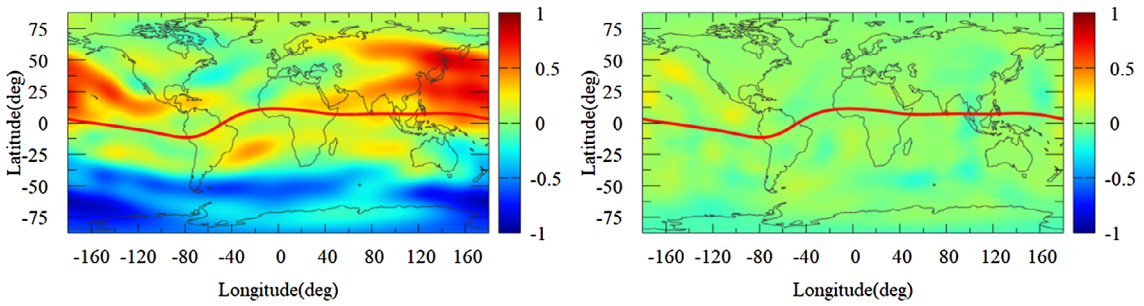

(a) Bias of SHPG - BUAG in 2009 (b) Bias of TVPG - BUAG in 2009

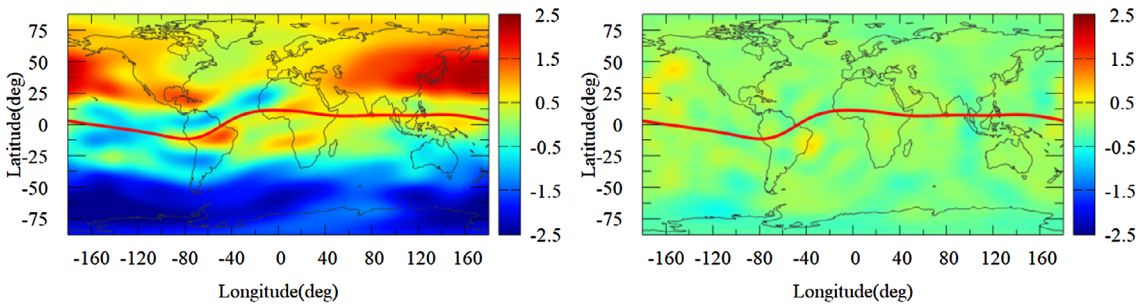

(c) Bias of SHPG - BUAG in 2014 (d) Bias of TVPG - BUAG in 2014

Fig. 5 Latitudinal and longitudinal bias for comparison between the forecast GIMs (SHPG and TVPG) and final daily GIMs BUAG in 2009 and 2014 (unit: TECU)

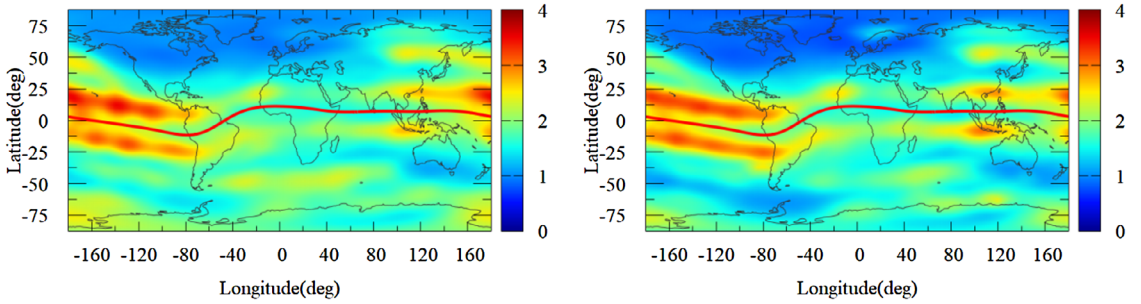

(a) RMS of SHPG - BUAG in 2009 (b) RMS of TVPG - BUAG in 2009

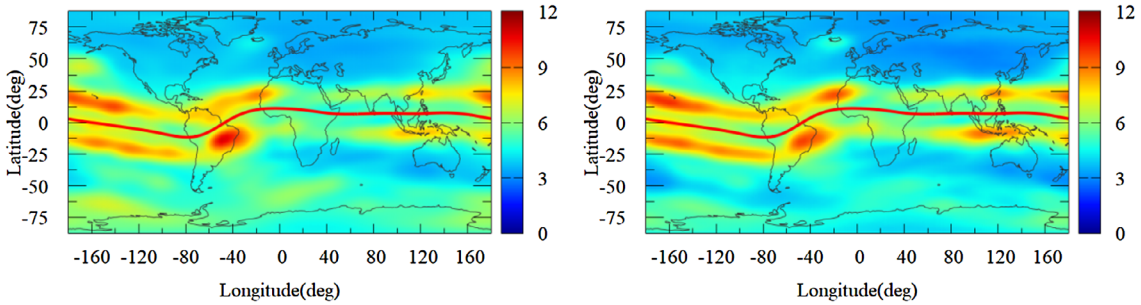

(c) RMS of SHPG - BUAG in 2014 (d) RMS of TVPG - BUAG in 2014

Fig. 6 Latitudinal and longitudinal RMS for comparison between the forecast GIMs (SHPG and TVPG) and final daily GIMs BUAG in 2009 and 2014 (unit: TECU)

between forecast GIMs and BUAG in the middle and high latitudes of the Northern Hemisphere, as well as a few parts of mid-to-high latitudes of the Southern Hemisphere. However, there also is an apparent discrepancy between forecast GIMs and BUAG in the EIA region, especially over the middle of the Pacific Ocean. Furthermore, there are a few RMS values larger than ten TECU over these areas at high solar activity. Overall, the performance of forecast GIMs is significantly lower in low latitudes than that in middle and high latitudes.

3.3 Comparison with PPP derived VTEC

This section investigates the performance of the forecast GIMs by comparing them with PPP derived VTEC values in terms of daily and latitudinal behavior. Figures 7 and 8 present the bias and RMS values of the differences between GIMs (SHPG, TVPG, and BUAG) and PPPG on a daily basis and a latitudinal basis in 2009 and 2014, respectively. For the daily bias shown in Fig. 7 there are no obvious systematic errors between GIMs (SHPG, TVPG, and BUAG) and PPPG. The bias values for comparison between BUAG and PPPG are very stable, and nearly up to zero at both low and high solar activity. The forecast GIMs SHPG and TVPG show similar differences with PPPG. Apparently the differences are larger in 2014 than those in 2009. Also the daily RMS values indicate that there is an excellent consistency between BUAG and PPPG, with an annual mean of approximately 1.2 TECU in 2009 and less than three TECU in 2014, respectively. There are also only small discrepancies between forecast GIMs and PPPG, with annual mean RMS values of less than two TECU in 2009. At high solar activity the daily RMS values show significant fluctuations with the seasons. The forecast GIMs (SHPG and TVPG) have a relatively larger discrepancy with PPPG, especially during northern spring with several RMS values larger than eight TECU.

In order to test the detailed performance, we also investigate the latitudinal differences between GIMs and PPPG. The bias and RMS values are presented in Fig. 8. In 2009 the bias values show that GIMs underestimate VTEC values over most of the latitudes, except low latitudes and a few part of middle southern latitudes. In 2014 TVPG and BUAG overestimate VTEC values in the EIA region and a few southern latitudes. Meanwhile, SHPG overestimate VTEC values in northern latitudes and underestimate those in southern latitudes. Generally, TVPG and BUAG have similar bias values when comparing with PPPG in 2009 and 2014. SHPG significantly underestimate VTEC values in middle and high latitude of Southern Hemisphere. Additionally, RMS values indicate that there is an excellent consistency between GIMs and PPPG in the middle and high latitudes, especially at low solar activity. Also, when compared to forecast GIMs, the final daily GIMs BUAG obvi-

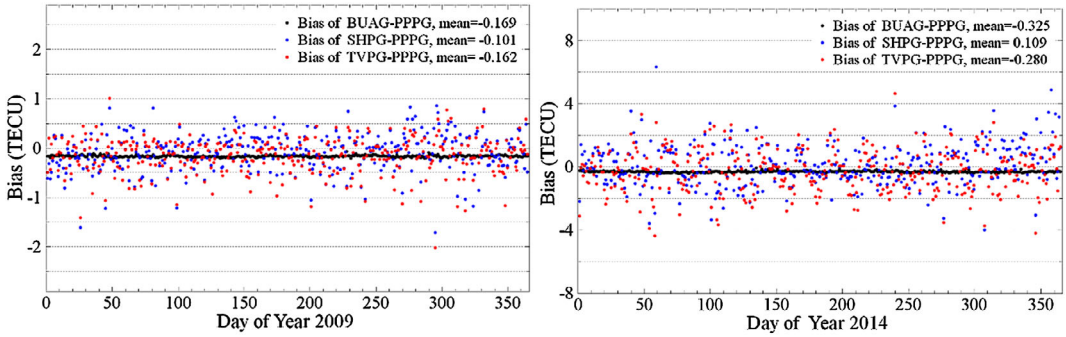

(a) Daily bias for comparison between GIMs and PPPG

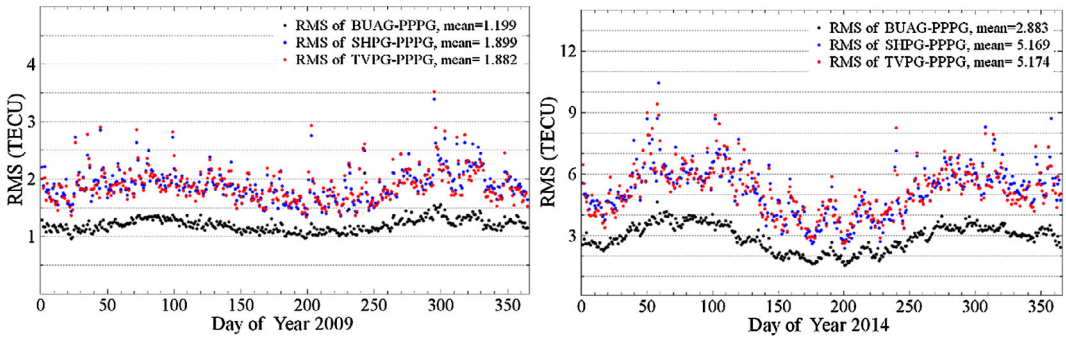

(b) Daily RMS for comparison between GIMs and PPPG

Fig. 7 Differences between GIMs (SHPG, TVPG and BUAG) and PPP derived VTEC in 2009 and 2014

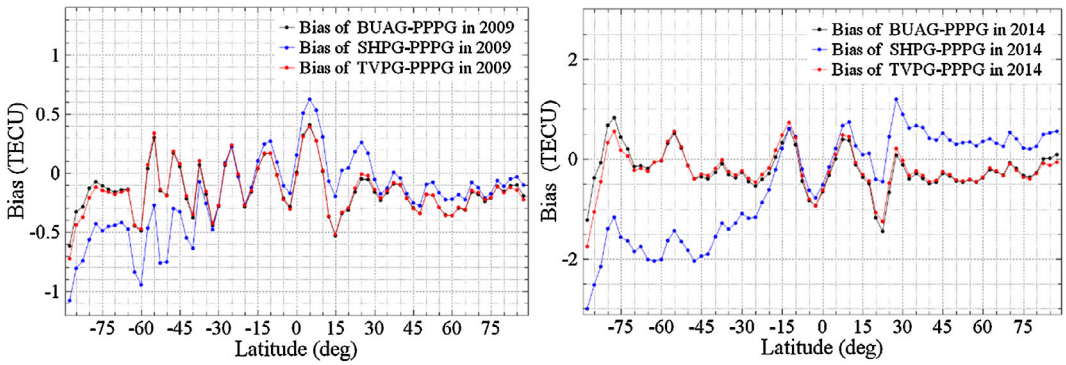

(a) Latitudinal bias for comparison between GIMs and PPPG

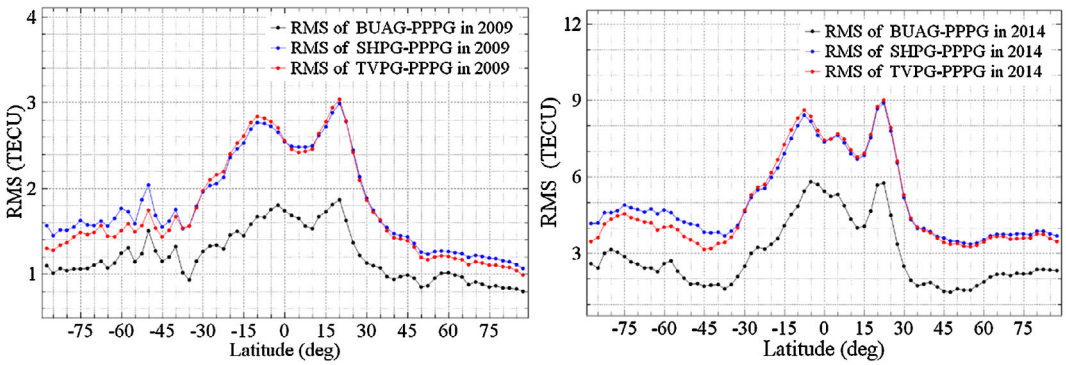

(b) Latitudinal RMS for comparison between GIMs and PPPG

Fig. 8 Latitudinal differences between GIMs (SHPG, TVPG and BUAG) and PPP derived VTEC in 2009 and 2014

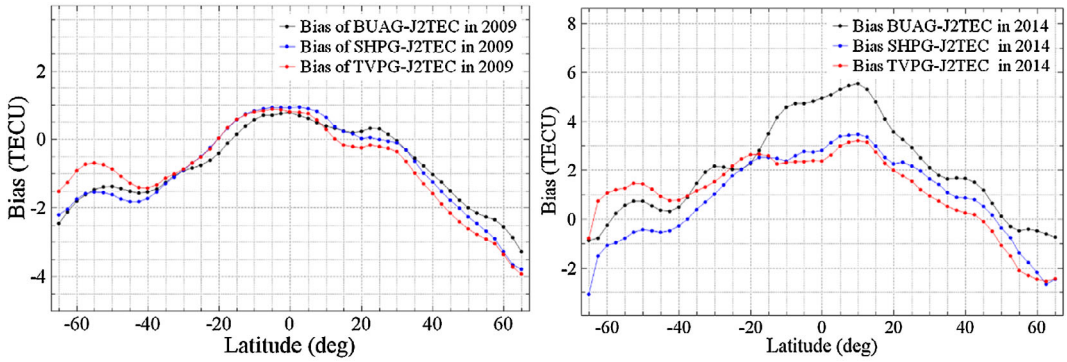

(a) Latitudinal bias for comparison between GIMs and J2TEC

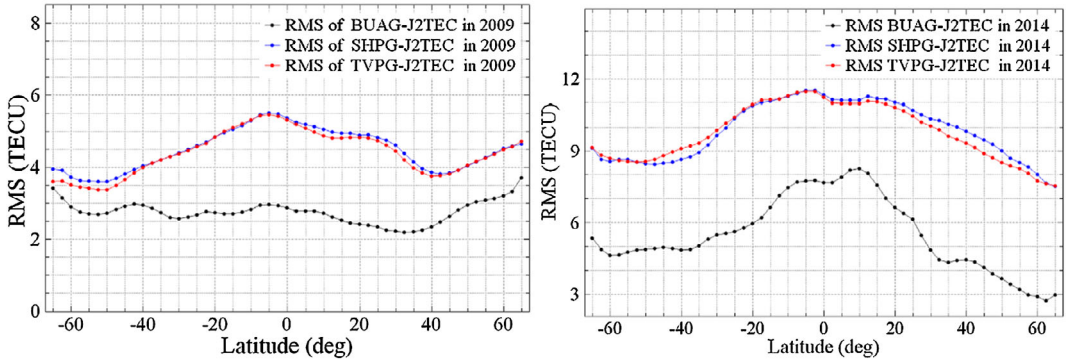

(b) Latitudinal RMS for comparison between GIMs and J2TEC

Fig. 9 Latitudinal differences between GIMs (SHPG, TVPG and BUAG) and JASON-2 VTEC in 2009 and 2014

ously have better consistency with PPPG at all latitudes. In 2009 TVPG have slightly better consistency with PPPG in mid-to-high and high latitudes. At high solar activity SHPG and TVPG have a similar performance in northern latitudes and low southern latitudes. Overall, both forecast GIMs and final daily GIMs have relatively low accuracy in low latitudes. Thus, the poor performance of forecast GIMs does not have much to do with the forecast algorithms, but is due to the basic VTEC dataset with low accuracy in low latitudes (Wang et al. 2020).

3.4 Comparison with JASON-2 VTEC

The JASON-2 altimeter provides independent VTEC measurements, which form a good resource for evaluating the accuracy of GIMs over oceans. Figure 9 shows the latitudinal bias and RMS values for comparison between both forecast GIMs (SHPG and TVPG) and final daily GIMs BUAG and JASON-2 VTEC. According to the bias shown in Fig. 9, both forecast GIMs and final daily GIMs are smaller than JASON-2 VTEC in low-middle and high latitudes at low solar activity. Theoretically JASON-2 VTEC should be smaller than GIMs. This is because JASON-2 VTEC only observes heights from the bottom of ionosphere to the JASON satellite orbit at an altitude of about 1300 km. GNSS derived GIMs generally include the plasmaspheric electron content contribution, which covers heights from the topside of the ionosphere to the GNSS satellite orbit at an altitude beyond 20,000 km. Thus, there might be a systematic error between J2TEC and GNSS derived GIMs (Mandrake et al. 2005; García-Rigo et al. 2011; Wang et al. 2018b). Although VTEC values would be larger at high solar activity, in 2014 both forecast GIMs and final daily GIMs are still smaller than J2TEC at mid-high latitudes. Generally, the latitudinal bias values that compare GIMs and J2TEC show a similar trend in 2009; again showing no significant differences. In 2014 the bias between BUAG and J2TEC are obviously larger in low latitudes than that between forecast GIMs and J2TEC. Therefore, it is difficult to determine the performance of forecast GIMs by only investigating latitudinal bias values.

According to the latitudinal RMS values shown in Fig. 9, the final daily GIMs BUAG have the best consistency with J2TEC at both low and high solar activity. In 2009 the relatively stable RMS values indicate that the differences between BUAG and J2TEC in different latitudes are not significant. There is an obvious discrepancy between BUAG and J2TEC in low latitudes in 2014. At high solar activity there is relatively better consistency between BUAG and J2TEC in middle and high latitudes of Northern Hemisphere than

that in southern latitudes. At the same time in 2009 there is slightly better consistency between TVPG and J2TEC in low and low-middle latitudes of Northern Hemisphere and middle and mid-high latitudes of Southern Hemisphere. In 2014 TVPG have slightly better consistency with J2TEC in northern latitudes and slightly poorer consistency with J2TEC in middle southern latitudes, with respect to SHPG. When compared to the final daily GIMs, the forecast GIMs have an obvious larger discrepancy with J2TEC at both low and high solar activity. On the one hand, the final daily GIMs might have low accuracy due to the lack of GNSS observations over oceans. On the other hand, extrapolation of GIMs over these areas would further enlarge the errors. Thus, the forecast GIMs apparently show a large discrepancy with J2TEC, especially at high solar activity.

4 Discussion

From the comparative results, the forecasting GIMs TVPG based on an adaptive AR modeling of grid point VTEC values perform obviously better than the SHPG. At the algorithmic level, the similarities between these two kinds of forecasting GIMs is that both of them are based on adaptive AR modeling. The most basic difference is that the input data used for forecasting TVPG and SHPG are the time series of VTEC values and SH coefficients, respectively. For forecasting SHPG, the errors of predicted SH coefficients would have negative impacts on VTEC predictions of all grid points. While, for TVPG, the VTEC values of each grid point are predicted independently. Certainly, the performance of forecasted GIMs over different regions are quite different due to the geographic distribution of GNSS stations as well as the different solar and geomagnetic activities. The precision of the original input data (final GIMs) is not the same at each grid point. It would make the precision of the forecasted GIMs is not the same either in different areas. As seen in Fig. 6, the performance of forecasted GIMs is basically better in middle and high northern latitudes than in those latitudes of the Southern Hemisphere. Also, there is obviously better consistency between forecasted GIMs and final GIMs during low solar activity. In addition, the upper atmospheric wind field might be another important factor, which has a great influence on the neutral composition and O/N_2 ratio (Bhuyan and Borah 2007; Olwendo et al. 2013). The O/N_2 ratio plays an important role in driving the TEC values variation in different seasons. Compared to summer months, the higher O/N_2 ratio would occur in the winter months during high solar activity (Bagiya et al. 2009). TEC increases as the O/N2 ratio increases. Because the N2 dissociation has a great influence on the process of removing the ambient electrons. The decrease of N2 would result in higher electron densities. In addition, vertical winds are downward (upward) in the winter (summer) hemisphere, resulting in increase (decrease) of the O/N2 ratio. Consequently, weaker recombination leads to higher TEC in the winter hemisphere (Bhuyan and Borah 2007; Olwendo et al. 2013). The daily RMS values in Fig. 3 and Fig. 7 have indicated that the performance of forecasting is apparently related to seasons. Besides, the RMS values show an obvious intraseasonal oscillation of about $20 \sim 30$ days in 2014. It might be related to the 27-day solar rotational cycle. This intraseasonal oscillation occurs not only between forecasted GIMs and final GIMs but also among different final GIMs from different analysis centers (Wang et al. 2016). In addition, there are kinds of factors (geophysical conditions, solar activity, neutral wind, storm-time equatorward winds, and O/N2 ratio etc.) which affect the VTEC variations in low latitudes, especially in the EIA region. The EIA is formed mainly from the removal of plasma from the around equator by the upward $E \times B$ drift with small accumulations when the crests are within approximately $\pm 20^\circ$ magnetic latitudes and no accumulation when they are beyond approximately $\pm 25^\circ$ magnetic latitudes (Balan et al. 2018). The development of EIA requires the upward drift velocity which depends on various geophysical conditions especially solar activity with smaller drift for lower levels of solar activity. The neutral wind plays an important role in the asymmetric structure of the EIA region. During the recovery phase of geomagnetic storms, the storm-time equatorward winds lead to negative storms. During this time, EIA sometimes gets inhibited with a peak in density at the equator (Balan et al. 2018). Furthermore, the strength of the equatorial electrojet (EEJ) affects the ionization in the equatorial anomaly region. Also, strong EEJ might bring more effects with extension to latitudes beyond the EIA region. Many studies indicated the positive correlation of TEC values and EEJ earlier (Rastogi et al. 1979; Sethia et al. 1980; Dabas et al. 1984; Bhuyan et al. 2003). At the same time, the input data GIMs is basically generated by using mathematical fitting model without physical information (Hernández-Pajares et al. 2009; Roma-Dollase et al. 2018a). Therefore, Fig. 8 shows the performances of both daily final GIMs and forecasted GIMs are greatly limited over low latitudes. In general, according to the daily and latitudinal RMS values presented above, the greater VTEC values due to various factors would lead to larger RMS values at different time and locations.

5 Conclusions

For achieving sub-meter accuracy for single-frequency users, short-time forecasting of GIMs would be an important approach for providing a basic background model for real-time GNSS applications, such as the navigation for autonomous vehicle, positioning for agricultural machinery in

precision agriculture, as well as management of intelligent transportation. GNSS deeply affects human future life, has tremendous applicable value, especially the high precision positioning and navigation. As one of the most important error resources, the ionospheric delay errors have a great impact on GNSS. Better forecast GIMs would improve the performance of the real-time GNSS positioning in various aspects of human life. An adaptive autoregressive model of SH coefficients was proposed to forecast GIMs. However, VTEC forecasts based on SH coefficients would introduce twice accumulated errors. In this study, an improved algorithm is proposed to forecast GIMs based on VTEC values, which has only once accumulated error. Two kinds of forecast GIMs (SHPG and TVPG) are generated from the SH coefficients and grid point VTEC values, respectively. To assess the performance of the forecast GIMs comparisons and validations are conducted using final daily GIMs and PPP-derived VTEC values, as well as JASON-2 VTEC. The comparative results show that SHPG overestimate VTEC values in northern latitudes and underestimate VTEC values in southern latitudes. According to the latitudinal bias shown in Figs. 3 and 4, there is no obvious overestimation or underestimation for TVPG. With respect to the final daily GIMs BUAG, the performance of TVPG is apparently better in middle and high latitudes than that of SHPG at both low and high solar activity. Additionally, by comparing with PPP derived VTEC, the final daily GIMs BUAG have relatively low accuracy in low latitudes, especially at high solar activity. Thus, the forecast GIMs SHPG and TVPG also show an obviously large discrepancy with respect to PPP-derived VTEC values. Compared to SHPG, TVPG have a little better consistency with PPPG in middle and high latitudes of northern hemisphere, and have slightly better consistency with PPPG in middle and high latitudes of Southern Hemisphere. Furthermore, by comparison with JASON-2 VTEC, there are stable differences between BUAG and J2TEC in different latitudes at low solar activity. In 2014, there is an obvious discrepancy between BUAG and J2TEC in low latitudes due to the high solar activity. When compared to SHPG, TVPG have slightly better consistencies with J2TEC in low and high latitudes of northern hemisphere and mid-high latitudes of southern hemisphere at low solar activity, as well as in northern latitudes at high solar activity.

In general, the proposed method for forecasting GIMs is based on an adaptive AR modeling of grid point VTEC values, and it is essentially better than the AARM method which is based on the extrapolation of SH coefficients. However, it is still a great challenge to improve the performance of daily GIMs in low latitudes. This is a key problem affecting seriously the performance of the forecast GIMs in low latitudes. In addition, physical information in terms of solar and geomagnetic activities, as well as the neutral wind of the upper atmosphere, might be introduced in global ionospheric modeling and forecasting in the further studies. Additionally, the proposed method is basically tested with final GIMs as the fundamental input data. While in an operational scenario, the forecasting should require rapid GIMs in a short period of time. We would like to provide the stable forecasting GIMs products after adequate testing in the near future.

Acknowledgements The authors would like to thank IGS for providing GNSS data and NASA/CNES for JASON data. This study has been funded by the National Natural Science Foundation of China (No. 41804026, No. 41804024 and No. 41931075) and the National Key Research and Development Program of China (No. 2017YFB0503401).

Conflicts of Interest The authors declare no conflict of interest.

References

Angrisano, A., Gaglione, S., Gioia, C., Massaro, M., Robustelli, U.: Assessment of NeQuick ionospheric model for Galileo single-frequency users. Acta Geophys. **61**(6), 1457–1476 (2013)

Bagiya, M.S., Joshi, H., Iyer, K., Aggarwal, M., Ravindran, S., Pathan, B.: TEC variations during low solar activity period (2005–2007) near the equatorial ionospheric anomaly crest region in India. Ann. Geophys. **27**, 1047–1057 (2009)

Balan, N., Souza, J., Bailey, G.: Recent developments in the understanding of equatorial ionization anomaly: a review. J. Atmos. Sol.-Terr. Phys. **171**, 3–11 (2018)

Bhuyan, P., Borah, R.R.: TEC derived from GPS network in India and comparison with the IRI. Adv. Space Res. **39**(5), 830–840 (2007)

Bhuyan, P., Chamua, M., Bhuyan, K., Subrahmanyam, P., Garg, S.: Diurnal, seasonal and latitudinal variation of electron density in the topside F-region of the Indian zone ionosphere at solar minimum and comparison with the IRI. J. Atmos. Sol.-Terr. Phys. **65**(3), 359–368 (2003)

Bilitza, D.: International reference ionosphere 2000. Radio Sci. **36**(2), 261–275 (2001)

Bilitza, D., Reinisch, B.W.: International reference ionosphere 2007: improvements and new parameters. Adv. Space Res. **42**(4), 599–609 (2008)

Bilitza, D., Rawer, K., Bossy, L.: International reference ionosphere 1990. Planet. Space Sci. **40**(4), 544 (1992)

Bilitza, D., McKinnell, L.-A., Reinisch, B., Fuller-Rowell, T.: The international reference ionosphere today and in the future. J. Geod. **85**(12), 909–920 (2011)

Bilitza, D., Altadill, D., Truhlik, V., Shubin, V., Galkin, I., Reinisch, B., Huang, X.: International reference ionosphere 2016: from ionospheric climate to real-time weather predictions. Space Weather **15**(2), 418–429 (2017)

Cheng, H.: Autoregressive modeling and causal ordering of economic variables. J. Econ. Dyn. Control **4**(3), 243–259 (1982)

Costa, A.H., Hengstler, S.: Adaptive time–frequency analysis based on autoregressive modeling. Signal Process. **91**(4), 740–749 (2011)

Dabas, R., Bhuyan, P., Tyagi, T., Bhardwaj, R., Lal, J.: Day-to-day changes in ionospheric electron content at low latitudes. Radio Sci. **19**(3), 749–756 (1984)

De Franceschi, G., Zolesi, B.: Regional ionospheric mapping and modelling over Antarctica. Ann. Geophys. **41**(5–6), 813–8181 (1998)

Feltens, J., Schaer, S.: IGS products for the ionosphere. In: IGS Analysis Centers Workshop, pp. 1–7 (1998)

García-Rigo, A., Monte, E., Hernández-Pajares, M., Juan, J.M., Sanz, J., Aragón-Angel, A., Salazar, D.: Global prediction of the vertical total electron content of the ionosphere based on GPS data. Radio Sci. **46**(6), RS0D25 (2011)

Gu, X., Jiang, J.: A complex autoregressive model and application to monthly temperature forecasts. Ann. Geophys. **23**(10), 3229–3235 (2005)

Hamilton, J.D.: Time Series Analysis. Princeton University Press, Princeton (1994)

Hernández-Pajares, M., Juan, J., Sanz, J.: New approaches in global ionospheric determination using ground GPS data. J. Atmos. Sol.-Terr. Phys. **61**(16), 1237–1247 (1999)

Hernández-Pajares, M., Juan, J., Sanz, J., Orus, R., Garcia-Rigo, A., Feltens, J., Komjathy, A., Schaer, S., Krankowski, A.: The IGS VTEC maps: a reliable source of ionospheric information since 1998. J. Geod. **83**(3–4), 263–275 (2009)

Hernández-Pajares, M., Roma-Dollase, D., Krankowski, A., García-Rigo, A., Orús-Pérez, R.: Methodology and consistency of slant and vertical assessments for ionospheric electron content models. J. Geod. **91**(2), 1–10 (2017)

Karthik, P., Ratnam, D.V., Vanga, N., Brahmanadam, P., Rao, B.S.S., Kumar, K.S.: Auto regressive ionospheric prediction model for GPS applications. Int. J. Comput. Appl. **48**(4), 7–9 (2012)

Klobuchar, J.: Ionospheric time-delay algorithm for single-frequency GPS users. IEEE Trans. Aerosp. Electron. Syst. **3**, 325–331 (1987)

Komjathy, A.: Global Ionospheric Total Electron Content Mapping Using the Global Positioning System. University of New Brunswick, Fredericton (1997)

Krankowski, A., Kosek, W., Baran, L.W., Popinski, W.: Wavelet analysis and forecasting of VTEC obtained with GPS observations over European latitudes. J. Atmos. Sol.-Terr. Phys. **67**(12), 1147–1156 (2005)

Lee, C.Y., Tippett, M.K., Sobel, A.H., Camargo, S.J.: Autoregressive modeling for tropical cyclone intensity climatology. J. Climate (2016). https://doi.org/10.1175/JCLI-D-15-0909.1

Li, Z., Yuan, Y., Wang, N., Hernandez-Pajares, M., Huo, X.: SHPTS: towards a new method for generating precise global ionospheric TEC map based on spherical harmonic and generalized trigonometric series functions. J. Geod. **89**(4), 331–345 (2015)

Liu, T., Zhang, B., Yuan, Y., Li, M.: Real-Time Precise Point Positioning (RTPPP) with raw observations and its application in real-time regional ionospheric VTEC modeling. J. Geod. **1**, 1–17 (2018)

Mandrake, L., Wilson, B., Wang, C., Hajj, G., Mannucci, A., Pi, X.: A performance evaluation of the operational Jet Propulsion Laboratory/University of Southern California global assimilation ionospheric model (JPL/USC GAIM). J. Geophys. Res. Space Phys. **110**, A12 (2005)

Mannucci, A., Wilson, B., Yuan, D., Ho, C., Lindqwister, U., Runge, T.: Global mapping technique for GPS-derived ionospheric total electron content measurements. Radio Sci. **33**(3), 565–582 (1998)

Nava, B., Coïsson, P., Radicella, S.M.: A new version of the NeQuick ionosphere electron density model. J. Atmos. Sol.-Terr. Phys. **70**(15), 1856–1862 (2008)

Nigussie, M., Radicella, S., Damtie, B., Nava, B., Yizengaw, E., Groves, K.: Validation of the NeQuick 2 and IRI-2007 models in East-African equatorial region. J. Atmos. Sol.-Terr. Phys. **102**, 26–33 (2013)

Olwendo, O., Baki, P., Cilliers, P., Mito, C., Doherty, P.: Comparison of GPS TEC variations with IRI-2007 TEC prediction at equatorial latitudes during a low solar activity (2009–2011) phase over the Kenyan region. Adv. Space Res. **52**(10), 1770–1779 (2013)

Orús, R., Hernández-Pajares, M., Juan, J., Sanz, J.: Improvement of global ionospheric VTEC maps by using kriging interpolation technique. J. Atmos. Sol.-Terr. Phys. **67**(16), 1598–1609 (2005)

Prieto-Cerdeira, R., Orús-Pérez, R., Breeuwer, E., Lucas-Rodriguez, R., Falcone, M.: Performance of the Galileo single-frequency ionospheric correction during in-orbit validation. GPS World **25**(6), 53–58 (2014)

Rastogi, R., Sethia, G., Chandra, H., Deshpande, M., Davies, K., Murthy, B.: Total electron content and F-region electron density distribution near the magnetic equator in India. J. Atmos. Terr. Phys. **41**(6), 561–564 (1979)

Roma-Dollase, D., Hernández-Pajares, M., Krankowski, A., Kotulak, K., Ghoddousi-Fard, R., Yuan, Y., Li, Z., Zhang, H., Shi, C., Wang, C.: Consistency of seven different GNSS global ionospheric mapping techniques during one solar cycle. J. Geod. **92**, 691–706 (2018a)

Roma-Dollase, D., Hernández-Pajares, M., Krankowski, A., Kotulak, K., Ghoddousi-Fard, R., Yuan, Y., Li, Z., Zhang, H., Shi, C., Wang, C.: Consistency of seven different GNSS global ionospheric mapping techniques during one solar cycle. J. Geod. **92**(6), 691–706 (2018b)

Schaer, S.: Mapping and Predicting the Earth's Ionosphere Using the Global Positioning System. Geod.-Geophys., vol. 59 (1999)

Sethia, G., Rastogi, R., Deshpande, M., Chandra, H.: Equatorial electrojet control of the low latitude ionosphere. J. Geomagn. Geoelectr. **32**(4), 207–216 (1980)

Shi, C., Gu, S., Lou, Y., Ge, M.: An improved approach to model ionospheric delays for single-frequency precise point positioning. Adv. Space Res. **49**(12), 1698–1708 (2012)

Tulunay, E., Senalp, E.T., Radicella, S.M., Tulunay, Y.: Forecasting total electron content maps by neural network technique. Radio Sci. **41**(4), 1–32 (2006)

Wang, C., Shi, C., Zhang, H., Fan, L.: Improvement of global ionospheric VTEC maps using the IRI 2012 ionospheric empirical model. J. Atmos. Sol.-Terr. Phys. **146**, 186–193 (2016)

Wang, C., Shi, C., Fan, L., Zhang, H.: Improved modeling of global ionospheric total electron content using prior information. Remote Sens. **10**(1), 63 (2018a)

Wang, C., Xin, S., Liu, X., Shi, C., Fan, L.: Prediction of global ionospheric VTEC maps using an adaptive autoregressive model. Earth Planets Space **70**(1), 18 (2018b)

Wang, C., Fan, L., Wang, Z., Shi, C.: Assessment of global ionospheric maps over continental areas using precise point positioning technique. J. Spat. Sci. **65**, 25–39 (2020)

Weiss, J., Bernardara, P., Andreewsky, M., Benoit, M.: Seasonal autoregressive modeling of a skew storm surge series. Ocean Model. **47**(3), 41–54 (2012)

Zhang, B.C., Yuan, Y.B., Li, Z.S., Ou, J.K.: Extraction of line-of-sight ionospheric observables from GPS data using precise point positioning. Sci. China Earth Sci. **55**(11), 1919–1928 (2012)

Zhang, H., Xu, P., Han, W., Ge, M., Shi, C.: Eliminating negative VTEC in global ionosphere maps using inequality-constrained least squares. Adv. Space Res. **51**(6), 988–1000 (2013)

Zhang, B., Teunissen, P.J.G., Yuan, Y., Zhang, H., Li, M.: Joint estimation of vertical total electron content (VTEC) and satellite differential code biases (SDCBs) using low-cost receivers. J. Geod. **92**(4), 1–13 (2018)